Journal of Hydrology (2006) **xxx**, xxx–xxx

available at www.sciencedirect.com

SCIENCE DIRECT®

journal homepage: www.elsevier.com/locate/jhydrol

Multifractal large number of drops limit in rain

M. Lilley [a,1], S. Lovejoy [a,*], N. Desaulniers-Soucy [b,2], D. Schertzer [c,3]

[a] *Department of Physics, McGill University, 3600 University St., Montreal, Que., Canada H3A-2T8*
[b] *Advantech Satellite Networks, 2341 boul. Alfred-Nobel, 4e étage, Saint-Laurent, Qué., Canada H4S 2A9*
[c] *Laboratoire de Modélisation en Mécanique, case 162, Université Pierre et Marie Curie, 4, Place Jussieu, F-75252, Paris Cedex 5, France*

Received 31 October 2002; received in revised form 11 November 2003; accepted 30 November 2005

Summary Rain-drop size and position data were obtained for five different storms in the *HYDROP* (*HY*drometeor *D*etection and *R*anging using stere*O*-*P*hotography) experiment [Desaulniers-Soucy, N., 1999. Empirical test of the multifractal continuum in rain, Ph.D. thesis, McGill University, Montréal; Desaulniers-Soucy, N., Lovejoy, S., Schertzer, D., 2001. The HYDROP experiment: an empirical method for the determination of the continuum limit in rain. Atmos. Res. 59–60, 163–197]. The data from 18 scenes of an region $\approx 8\ m^3$ each containing 5000–15,000 rain drops were systematically and statistically analyzed in spheres ranging from 10 cm to 2 m in diameter. In four of the five storms, we found convincing evidence for the convergence to a multifractal scaling limit as the number of drops (N) per sphere was increased; the observed scaling exponents were quite close to those reported in the rain literature at much larger scales. By randomizing the positions of the drops, we directly compared the true fluctuation statistics with those of the classical theory; the fluctuations in the latter were significantly smaller. Careful consideration of the meteorological conditions, in particular the turbulence intensity and the drop size distributions, explained the observed variations in the scale of convergence to the multifractal regime.

* Corresponding author. Fax: +1 514 398 8434.
E-mail addresses: lilleym@physics.mcgill.ca (M. Lilley), lovejoy@physics.mcgill.ca (S. Lovejoy), Desaulniers-Soucy.N@ems-t.ca (N. Desaulniers-Soucy), schertze@cereve.enpc.fr (D. Schertzer).
[1] Fax: +1 514 398 8434.
[2] Fax: +1 514 335 3046.
[3] On leave to: Ecole Nationale des Ponts et Chaussées (CEREVE), 6-8, ave Blaise Pascal, Cité Descartes, 77455 Marne-la-Vallée, Cedex, France. Fax: +33 1 64 15 37 64.

Introduction

The large *N* limit in rain

Although clouds and precipitation are composed of particles, with few exceptions, meteorologists and hydrologists

0022-1694/$ - see front matter
doi:10.1016/j.jhydrol.2005.11.063

are concerned with large numbers N of such particles. In much the same way as standard continuum mechanics treats molecules collectively ignoring their particulate nature, precipitation is usually treated as a continuous field. In standard treatments of fluid mechanics (e.g., Batchelor, 1970; Tritton, 1990 etc.), the classical continuum limit is graphically illustrated by considering an immaterial sphere of radius r filled with air, e.g., a sample of the atmosphere. For r small compared to the mean inter-molecular distance, there will be large fluctuations in properties such as mean density or velocity depending on whether zero, one, or several molecules are present inside the volume. As r and therefore N are progressively increased, the relative fluctuations become smaller (classically, they decrease as $N^{-1/2}$). In the atmosphere under standard conditions — even at scales of tens of microns — the continuum hypothesis for air accurately holds. However, due to turbulent variations in the macroscopic density, temperature, pressure, velocity, etc. at scales typically of the order of a millimeter to a centimeter, the mean will start to vary again. Nevertheless, there exists a range of scales (from microns to millimeters) over which the properties are independent of the radius r. This justifies the continuum hypothesis. By averaging over volumes whose radius is much larger than the microscale while simultaneously much smaller than the macroscale, the continuum hypothesis allows us to define the macroscopic continuum quantities.

In the same fashion, the assumption in cloud and precipitation physics has been that, in the large N limit, particle sizes, spatial distributions, rain/snow rates, and liquid water content (LWC) are classical continua. This has many implications including the prediction that, for large enough samples, the spatial distribution should be Poissonian and that the drop size statistics should be independent of the measuring volumes. In spite of its important implications in cloud and rain modeling and measurement — although it is partly linked to experimental difficulties — only limited effort has been made towards a systematic experimental test of this assumption. This is true even though, simply due to the effects of turbulence, the existence of a classical continuum in rain is far from evident. Indeed, from the largest scales on down, it is not obvious that homogeneity is ever reached even at small scales of the order of the typical inter-drop distance.

Precipitation is strongly coupled to the wind field which is itself highly turbulent (see, e.g. Anselmet et al., 2001, for a recent review). Even in strong rain, the mean inter-drop distance is typically of the order of ten centimeters (see, e.g. the direct measurements below) and at least at the small scales, the wind is multifractal — the result of cascade processes concentrating energy and other fluxes unevenly into progressively smaller regions of space. One would therefore expect the precipitation to similarly exhibit a hierarchical clustering pattern at least down to a drop-size dependent inner scale where the inertia of the particles becomes important and where the drops ''decouple'' from the wind. In fact, starting in the early 1980s, this is exactly what has been found at larger scales — first fractal structures (e.g., rain perimeters, Lovejoy, 1982), and then multifractal statistics (e.g., Schertzer and Lovejoy, 1985, 1987; Lovejoy et al., 1987); see the review Lovejoy and Schertzer, 1995 and the quantitative intercomparison in ''Multifractal results in rain''.

Several types of rainfall and cloud analyses have been conducted in order to study the small scale properties of rain and clouds. Until now they have not been able to successfully investigate the large N limit by considering large enough N over a wide enough range of scales. Most of the relevant studies (mostly time series) have been made with disdrometers. More detailed reviews of the literature can be found in Desaulniers-Soucy (1999), Desaulniers-Soucy et al. (2001); here we only mention a few of the more relevant highlights in rain. Recent examples of the classical approach are Kostinski and Jameson (1997, 1999), Jameson and Kostinski (1998, 1999, 2000a,b, 2001, 2002), Jameson et al. (1999) and Uijlenhoet et al. (1999) who have used disdrometers to investigate the size distributions of raindrops and their corresponding times of arrival over narrow ranges of scales. Relevant studies using other measurement devices include Kozikowska et al. (1984), Paluch and Baumgardner (1989), Brenguier (1993), Malinowski and Zawadzki (1993). First — and most important — none of these studies have found evidence that pure Poisson behavior is a good description of rain statistics. On the contrary, they found systematic deviations from pure Poisson statistics in time series and in a few instances in spatial experiments. For example, Uijlenhoet et al. (1999) found a deviation from Poisson statistics for drops <1.14 mm, consistent with the intuitive idea of a decoupling of the largest drops from atmospheric dynamics at the smallest scales; Jameson et al. (1999) found clustering in drops over time scales of seconds to minutes. In spite of the existence of those systematic departures from Poisson statistics, the tendency has been to introduce correction models such as ''doubly stochastic Poisson process'', ''Poisson mixture'', and ''compound Poisson processes'' (e.g., Jameson and Kostinski, 1999) that attempt to account for departures in what could be called a ''scale-bound Poisson framework''. Such models are not appropriate for processes with heterogeneity over wide ranges of scales, so that it is not surprising that this literature has been mostly divorced from the scaling literature. Existing compound Poisson models are ad hoc in the sense that there is no underlying turbulent cloud theory which predicts them. They are introduced simply in an attempt to mimick the data over narrow ranges of scale. In contrast, cascade models are turbulence-based physical models albeit ''phenomenological'', which predict multifractal statistics from more basic considerations. These are conservation of fluxes, scale invariance and Fourier space locality of interactions (the dynamics mostly links scales which are not too different — hence the cascade phenomenology). These basic cascade properties are verifiable features of the dynamical (e.g., Navier–Stokes) equations. Multifractal compound Poisson models in which the number density of particles is Poisson but with space-time mean determined by a cascade process are compatible with turbulence and will be discussed elsewhere.

Very few small scale studies have attempted to systematically consider the statistics as functions of scale (see however Lovejoy et al. (2003) which is a very brief ''announcement'' of the results detailed here). At the drop scale, an early exception was a study by Lovejoy and Schertzer (1990) who investigated possible fractality of the support of rain (whether or not the support of rain is fractal, the rate in the raining regions can still be multifractal).

They used chemically treated blotting paper to record rain drop positions in a two-dimensional surface of 128^2 cm^2 and claimed evidence for fractal clustering of individual drop positions and liquid water with $D = 1.83$ (and codimension equal to $d - D = 0.17$, where $d = 2$ is the dimension of measuring space). Unfortunately, there were only 452 drops so it was concluded that larger scale studies were required (as underlined by Gabella et al., 2001). In spite of their limitations, these results were consistent: in Gabella et al. (2001), 16 simulations replicating the experiment lead to the conclusion that although the systematic and random errors in the blotting paper experiment limit the accuracy of the results, the non-fractal result $D = 2$ was unlikely ''since 2 realizations (out of 16) had $D < 1.84$, 6 had $D < 1.88$ and 13 had $D < 1.92$''. In support of these early results was a study by Lavergnat and Golé (1998) who found that the histograms of the arrival times of rain drops follow a power law (Pareto) behavior, which is a scaling distribution also implying hierarchical clustering of arrivals. Also relevant — although not quite at the drop scale — was the study of an $x - t$ rain section (a spatial cut evolving in time) at a 3 m, 0.1 s resolution (up to 540 m, 500 s) obtained with a lidar (Lovejoy and Schertzer, 1991), showing anisotropic multifractal space–time scaling of the high resolution lidar backscatter field. These three studies all confirmed the existence of scaling in various small scale rain statistics. Other relevant small scale scaling studies are those of cloud liquid water; Lovejoy and Schertzer (1995) and Davis et al. (1996) have shown that the cloud statistics are indeed multifractal down to at least 10 m.

In a recent paper, Fabry (1996) measured the acoustic noise produced by rain hitting an approximately 2 by 2 m sheet of metal. An analysis of the time series indicated a break somewhere around 1 s. This was interpreted as an indication that there was a characteristic time scale of ≈10 m in rain. This conclusion follows only if we follow Fabry and use an ad hoc drop velocity of 10 m s^{-1}. Had Fabry used instead a turbulent velocity to convert from time to space, he would have found a scale of 1 m (i.e., the scale of the sheet) implying that his measured time scale was simply the time corresponding to 1 m sized spatial structures and therefore was not a fundamental scale in rain.

Finally, we could mention another paper by Zawadski (1995) which interprets rain-drop time series from disdrometers. He estimates that the correlation codimension is ≈0.07 for drops smaller than 0.05 mm in diameter (in the same paper, good statistical scaling of effective radar reflectivity is obtained for a single radar scan over the spatial range 1–20 km).

The HYDROP experiment

The HYDROP stereophotographic experiment (Desaulniers-Soucy, 1999; Desaulniers-Soucy et al., 2001) is the most recent in a series of experiments aimed directly at investigating the large N limit in rain (homogeneous/classical or scaling/multifractal) over the range of several centimeters to several meters.

HYDROP used three adjacent nearly collinear Hasselblad cameras with 60 mm film. They were triggered near-simultaneously to reconstruct the three-dimensional rain-drop positions and size distributions using stereophotography. Two key empirical constraints were to be considered: (1) rain-drops fall relatively rapidly (up to 10 m s^{-1}, e.g., Beard, 1976); (2) the backscattered light intensity at the cameras is typically only 10^{-10} of the intensity incident on the rain-drop. The first constraint implies that in order to ''freeze'' the drops, the photographs had to be taken over very short time scales; the second constraint implies the use of very powerful light sources. To this end, a ≈50 μs time scale flash with two 1 kJ flashlamps was used. In addition, the camera shutter had to be open for a time of the order of 1/30 s — i.e., long enough to guarantee synchronization of the cameras with the flashes. This meant that the pictures had to be taken at night in order to minimize the background illumination. In order to match the film resolution of 6 μm and obtain a wide dynamic range of 12 bits of information per pixel, the resulting negatives were digitized using the scanning microdensitometer of the Dominion Astrophysical Observatory in Victoria. Since as many as 100,000 drops could be present on any given negative, the shape of each individual drop had to be parameterized as functions of projected image intensity distributions to make drop-matching between the negatives possible (see Desaulniers-Soucy, 1999 or Desaulniers-Soucy et al., 2001 for more details).

The exact geometry of the stereophotography was computed by first manually matching a set of roughly 50 drops across all three negatives and then reconstructing their three dimensional positions based on their two dimensional positions on each of the three negatives. This allowed regression algorithms to estimate the 20 odd projection matrix elements of the stereophotographic geometry, which allowed automatic matching of all the other drops based on their position and also on their intensity distribution parameters. Rain drop positions were determined to within ±3 mm in the lateral direction and ±3 cm in the depth of view direction. This uncertainty is somewhat smaller than the typical mean interdrop distance (≈10 cm) and does not significantly affect the statistics we discuss below, as they are over still larger distances. Since the drops act as lenses, the image of both light sources was clearly visible as two intensity peaks in the digital image of larger drops. The size of large rain drops was thus estimated by combining the angle subtended by the image of the intensity peaks on the rain-drop image and the estimate of its distance from the cameras. For smaller drops, the size was computed using the less accurate method based on the backscattered intensity, the inferred flashlamp illumination field and the drop position. Drop size was determined with an accuracy of ±0.25 mm for drops >1 mm and ±0.5 mm for drops <1 mm. The detection limit was 0.2 mm based on the resolution of the film used. Many other parameters were tuned to the same limit (e.g., diffraction and ''out of focus'' settings of the optics, the scanning resolution, etc.).

In order to optimize the experiment, different set-up geometries were tested. The size of the region of interest (ROI), which was the region (roughly) homogeneously lit (using custom-built parabolic reflectors) and in which raindrops were in sharp focus, was ≈8–10 m^3 varying slightly depending on the experimental lay-out used. Within the ROI, a total of between ≈5000 and ≈20,000 drops were reconstructed for each of the 18 realizations studied, obtained during five different rain events; this represented

roughly half the total number of drops whose positions were reconstructed, and all but 10% of potential drop image candidates within the ROI.

The remainder of the paper is structured as follows. In ''Theoretical overview'', we give a theoretical description of multifractals (''Properties of cascades: conservative multifractals'' and ''Geophysical fields and non-conservative multifractals''), we review the results obtained for the universal multifractal exponents obtained in previous studies of rain (''Multifractals results in rain'') and we contrast the predictions of the classical and multifractal statistics. In ''Description of the data sets'', we give a brief qualitative and meteorological description of the five rain events. In ''Analysis'', we introduce the method used to statistically investigate the nature of the large N limit. We then discuss the scaling of the statistical moments of particle size distribution and liquid water content and comment in detail on the effects of the particle size distributions on the scale of convergence to the large N limit (''The statistical analysis for increasing scales'' to ''Number, volume and (normalized) ηth power density drop size distributions and (mono) fractal drop distributions''). In ''Universal multifractal parameters'', we apply the universal multifractal model to each rain event to estimate the universal multifractal parameters for each rain event. Finally, in ''Implications of universality for the radar reflectivity factors Z ($\eta = 2$)'', we briefly discuss the implications for the radar reflectivity Z.

Theoretical overview

Properties of cascades: conservative multifractals

In theoretical terms, the wind field is often considered to be the solution of a complex set of coupled non-linear partial differential equations. Structures/eddies in these fields are non-linearly coupled over a wide range of scales. Since the non-linear terms in the dynamical equations conserve the flux of energy while effecting a scale invariant transfer to smaller scales, the wind exhibits scaling properties; the best known statistical behavior is the Kolmogorov $k^{-5/3}$ energy spectrum (where k is the wavenumber). The scaling is broken only at the large scales due to the energy injection/forcing mechanism and at the small scales due to molecular dissipation/viscosity. Although there are no comparable non-linear partial differential equations that describe the rain field — the latter is always ''parameterized'' — there is no reason to expect that rain breaks this scale invariant symmetry. However, this statement does not imply a one-to-one correspondence between the rain field and the wind field any more than the Corrsin—Obukhov law of passive scalar advection which implies a one-to-one correspondence between the scalar and the wind field. Indeed, the multifractal generalization of the Corrsin—Obukhov law involves two non-trivially coupled cascades, one for the energy flux and one for the passive scalar variance flux. Similarly, Schertzer and Lovejoy (1987) proposed that rain is the result of a precipitation cascade coupled to the dynamical (wind) cascade. The direct conceptual link between the dynamical equations and the (phenomenological) multiplicative cascade model is the scale by scale conservation of the energy ε and other fluxes by the non-linear terms. In multiplicative cascades, the conserved fluxes pass through the system from large scales down through to structures at increasingly smaller scales. The small scale structures are modulated multiplicatively by the larger scale structures in a scale invariant way. Note that it is the energy flux through an eddy which is a multiplicative random variable, not the size of the eddy itself as in Jameson and Kostinski (1999). The succession of weak and strong modulating factors renders the survival of structures more complex and leads to a wide range of intensities ε_λ for larger and larger scale ratios $\lambda = L/l$ (L is the largest available scale of the set and l is the scale of investigation). This corresponds to the appearance of a hierarchy of singularities γ that are the exponents of divergence of the intensities in the small scale limit (i.e., very large resolution limit). The total flux is conserved, in the sense that (on average) it is independent of scale, $\langle\varepsilon\rangle = 1$. The fraction of space occupied by a singularity of order γ has a (statistical) codimension $c(\gamma)$, i.e., the probability ''Pr'' of exceedance of a given threshold λ^γ is scaling:

$$\Pr(\varepsilon_\lambda \geqslant \lambda^\gamma) \approx \lambda^{-c(\gamma)} \tag{1}$$

The equality in Eq. (1) is to within slowly varying factors (such as logarithms). When $c(\gamma)$ is smaller than the dimension of the embedding space d, (almost surely) every region where ε_λ exceeds λ^γ has a fractal dimension $D(\gamma) = d - c(\gamma)$.

We can equivalently describe the statistical properties of a random variable by all of its statistical moments:

$$\langle\varepsilon_\lambda^q\rangle \propto \lambda^{K(q)} \tag{2a}$$

where $K(q)$ is the (convex) moment scaling function. In the very large λ limit, $\Pr(\varepsilon_\lambda \geqslant \lambda^\gamma)$ and $\langle\varepsilon_\lambda^q\rangle$ are related by a Mellin transform which reduces to a Legendre duality for the exponents $c(\gamma)$ and $K(q)$ (see e.g., Parisi and Frisch, 1985, for a development in a somewhat different context):

$$\begin{aligned} K(q) &= \max_\gamma(q\gamma - c(\gamma)) \\ c(\gamma) &= \max_q(q\gamma - K(q)) \end{aligned} \tag{2b}$$

The statistics will then depend on the resolution λ (i.e., the scale of the region $l = L/\lambda$) over which the statistics are taken and on the order of singularity γ (or equivalently its corresponding statistical moment q).

It is important to briefly discuss the meaning of the existence of a hierarchy of singularities, with particular emphasis on the rain rate (Schertzer et al., 2002). If rain is multifractal, then, contrary to usual assumptions, rain rate would not admit a density with respect to the usual volume measure in the small scale limit (in the very large λ limit). Therefore, it cannot be defined with the help of (almost everywhere) pointwise and continuous functions (the basis of stochastic point processes), but only as (multi-) singular measures. The latter do not fit in the classical framework of continuum mechanics, but seem rather to be the key ingredients of a new world of discontinuous mechanics. We must then expect the large N limit of rain-drops to be non-classical; the presence of fractal dimensions $0 < D(\gamma) < d$ (or codimensions $0 < c(\gamma) < d$) physically implies clustering at all scales: singularities occur by patches. The singularity clusters — i.e., fractions of a sample where $\varepsilon_\lambda \geqslant \lambda^\gamma$ — are sparser and sparser with increasing codimensions, i.e., increasing singularities and the extreme events correspond-

ing to $c \geqslant d$ are almost surely not present on a given sample (see Schertzer and Lovejoy, 1991, for discussion). Let us finally recall that rather generically, multifractal fields have such a singular behavior that there is a finite critical order q_D of divergence of statistical moments, beyond which all the (theoretical) statistical moments $q > q_D$ are infinite and their empirical estimates are spurious and depend sensitively on the sample size (c.f. various rain estimates reviewed in Lovejoy and Schertzer, 1995: empirically, it seems $q_D \approx 3$). This corresponds to the fact that the tail of the cumulative probability distribution has a power-law of exponent q_D (it also corresponds to a first order multifractal phase transition (Schertzer and Lovejoy, 1992)) (Added in press: work in progress also finds $q_D \approx 3$ for LWC estimated for spheres in the scaling regime; in addition the value $q_D = 3$ is theoretically predicted on the basis of compound multifractal Poisson models and dimensional analysis).

In principle, $K(q)$ or $c(\gamma)$ can be practically any convex function; this corresponds to an infinite number of unknown parameters. As argued in Schertzer and Lovejoy (1997), this means that without further information, multifractals would be unmanageable. However, in the framework of universal multifractals (Schertzer and Lovejoy, 1987), multifractal processes converge into a class of ''universal models'' described by only three parameters: the degree of multifractality α characterizing the curvature of $K(q)$, the codimension of the mean C_1 characterizing the sparseness of the mean field, and the non-conservation parameter H which is a measure of the non-conservation of the observable geophysical field (see ''Geophysical fields and non-conservative multifractals''). The moment scaling function $K(q)$ for a conservative universal multifractal is then given by:

$$K(q) = \frac{C_1}{\alpha - 1}(q^\alpha - q) \qquad 0 \leqslant \alpha < 1, 1 < \alpha \leqslant 2 \text{ and } 0 < q < q_D$$
$$K(q) = C_1 q \log q \text{ for } \alpha = 1 \text{ and } 0 < q < q_D \tag{3a}$$

where q_D is a critical order of moments discussed above. The corresponding codimension function is:

$$c(\gamma) = C_1 \left(\frac{\gamma}{C_1 \alpha'} + \frac{1}{\alpha} \right)^{\alpha'} ; \ \frac{1}{\alpha} + \frac{1}{\alpha'} = 1 \text{ and } \gamma_0 < \gamma < \gamma_D \tag{3b}$$

Here $0 \leqslant \alpha \leqslant 2$, $C_1 > 0$, $\gamma_0 = -\alpha'/C_1\alpha$ and γ_D are the singularities corresponding to moments $q = 0$ and $q = q_D$, respectively, and α is the Levy index of the generator of the multifractal. In the limit $\alpha \to 0$, $K(q)$ becomes linear, the system is monofractal (the so-called β-model, Frisch et al., 1978). When $\alpha = 2$, it is the log-normal multifractal, somewhat misnamed because of the divergence at q_D; the tail of the distribution is ''heavier'' than that of a perfect log-normal.

In rain, universality has in fact been invoked since the 1970s as in the standard ''law of proportional effects'' used notably by Lopez (1977). Lopez used the standard argument for lognormal distributions, namely that the rain rate is the outcome of many independent processes multiplicatively modulating each other. He then invoked the standard central limit theorem on the log of the factors (which will be additive), concluding that the resulting process is lognormal. The modern cascade argument for conservative cascades starts with the multiplicative factors modulating the larger scale conserved fluxes (see the following section for the relation of this to the observables including rain rate). To obtain a universal multifractal process, the basic law of proportional effects is then invoked but with several caveats. First, there is no reason to assume that the variance of the logs of the factors is finite so that the generalized central limit theorem must be used, leading to log-Levy distributions. Second — and this was the technically nontrivial point of the debate on multifractal universality (Schertzer and Lovejoy, 1997) – the singular limit of the process requires: (a) a study of universality over a finite range of scales and only then, (b) the consideration of the nontrivial small scale limit. Whereas (a) yields log-normal or log-Levy generators, (b) leads to processes which are no longer log-normal or log-Levy, although this terminology is still often used instead of the convenient ''universal multifractals''. Indeed, the small scale limit generally introduces a finite critical order of divergence of statistical moments q_D and therefore power law deviations from log-Levy distributions for extreme events.

Geophysical Fields and non-conservative multifractals

The observable geophysical fields are generally not conserved but instead the energy injected at the largest scales gets dissipated downscale. An observable field is therefore related to a corresponding conserved field (the direct result of a multiplicative cascade) by an additional scaling exponent H, the ''non-conservation parameter''. The classical example of this distinction is for the turbulent velocity shears Δv, where Kolmogorov scaling implies $\Delta v = \varepsilon^{1/3}\Delta x^H$ with $H = 1/3$ (ε is the energy flux). This implies that the mean absolute shear is $\langle |\Delta v| \rangle \propto \langle \varepsilon^{1/3} \rangle \Delta x^H$ which, contrary to ε, changes with scale Δx (although $\langle \varepsilon_\lambda \rangle \approx 1$ for all scales). To model these scale by scale non-conservative fields, Schertzer and Lovejoy (1987) proposed the ''fractionally integrated flux (FIF)'' model in which the non-conservative field is obtained from a conservative one (possibly raised to a power) by fractional integration (power law filter, power law convolution) of order H. This is the most general linear scaling transformation.

Although the empirical situation for the rain rate is still not clear — primarily due to the difficulty in estimating the statistics of low or zero rain rate events — it seems that H is quite low, e.g., Tessier et al. (1996) and De Lima (1998) find $H \approx -0.1$. In contrast, for cloud liquid water content (LWC), Lovejoy and Schertzer (1995) and Davis et al. (1996) have found robust results with $H \approx 0.3$ which is close to the value found for the fluctuations in the concentration of a passive scalar advected by the wind field (the theoretical value is $H = 1/3$ for the passive scalar in the well developed Corrsin–Obukhov theory). Also, Lilley et al. (2004) and Radkevich et al. (2006) find horizontal values $H \approx 0.33 \pm 0.01$ for both cirrus clouds and aerosols using lidar data (the value 0.60 ± 0.02 indicating scaling stratification was found in the vertical, close to the theoretical value 3/5). (Note added in press: when the spectrum of the HYDROP LWC is analysed it also shows $H \approx 1/3$ at the lower wavenumbers with a transition to a white noise spectrum at the higher wavenumbers, see further comments below). Moreover, since the values for C_1 in clouds (about 0.08) were found to be close to those

in wind (and in other passive scalar studies), it appears that the cloud field has statistics quite near those of passive scalars. In rain, at the very least, the value of H is significantly smaller than that found in clouds or passive scalars. The sensitivity of the inner scale in rain to the drop/dynamics coupling and the effect of drop inertia on the inner scale appears to be the basic difference between rain and clouds. While in clouds, the inner scale is comparable to the dissipation scale, in rain it is typically somewhat greater, allowing — due to the weakness of the small scale coupling — drops to move freely from one turbulent eddy to another.

Multifractal results in rain

Historically, the understanding of extreme variability in rain has provided an important stimulus for multifractals. The first explicit empirical estimates of dimension/codimension functions were in radar rainfall (Schertzer and Lovejoy, 1985), as was the investigation of multifractal universality classes (Schertzer and Lovejoy, 1987). Since then, there have been many studies of multifractal scaling in rain. Today, the literature is sufficiently large that we will not attempt a complete review (see however the early review by Lovejoy and Schertzer (1995) which includes theoretical developments). For empirical papers on multifractals and rain, we can refer the reader to the more precise quantifications in Tables 1 and 2, which give spatial and temporal characterizations, respectively (they are not necessarily the same). Additional (primarily empirical) papers on multifractals in rain are: Lovejoy et al. (1987), Lovejoy and Schertzer (1990), Cârsteanu and Foufoula-Georgiou (1996), Gupta and Waymire (1990, 1993), Hubert and Carbonnel (1989), Hubert et al. (1993), Hubert (1995), Ladoy et al. (1991, 1993), Menabde et al. (1997), Marsan et al. (1996), Olsson (1995, 1996), Over and Gupta (1994), Bendjouhdi et al. (1997), Harris et al. (2001), Venugopal et al. (1999). In the following, we will rapidly comment on a few of the quantitative characterizations of multifractality in rain which are relevant to the HYDROP results discussed in ''Conclusion''. In Tables 1 and 2, we have only included analyses where the authors provided estimates of α and C_1 since otherwise quantitative intercomparison of empirical $K(q)$ functions is difficult, if not impossible. The main points to note are (a) the relative robustness of α in the range 1.2—1.5 and C_1 in the range 0.1—0.2 in space, (b) the rather different values α in the range 0.3—0.6 and C_1 in the range 0.2—0.6 in time. In space, key empirical difficulties are the fractal nature of the measuring networks for gauge measurements (Tessier et al., 1994), and for radar estimates, the conversion from reflectivity to rain (Lovejoy et al., 1996). A problem affecting all estimates is that of poor estimates of the low or zero rain rate; this is particularly acute in time series where often (e.g., from tipping bucket gauges) the low and zero rain rate statistics are poorly estimated. This implies that the question of the fractality of the support of rain is still an open question. Is rain only multifractal on a fractal support outside of which the rain rate is exactly zero? Should we then consider two separate processes, one controlling where and when it rains, the other determining the rate on the non-zero part? Or should we consider only a single process which is truncated to zero below some low threshold? In light of these uncertainties, the relatively small spread in multifractal exponents is quite encouraging.

The classical and multifractal large N limits

The classical large N limit yields straightforward statistical results. It is usually assumed that the probability per unit volume of finding a particle is constant. This implies that the number in any volume S_λ (of volume $\mathrm{vol}S_\lambda$), at scale ratio λ, is therefore a Poisson random variable whose mean is proportional to $\mathrm{vol}S_\lambda$. If we make the usual cloud physics assumption that there exists a scale-independent particle size distribution, then this distribution is the only aspect which changes between different rains; hence, the classical focus of research on drop size distributions. Assuming the existence of the first two statistical moments of the particle size distribution ($\langle v\rangle$, $\langle v^2\rangle$ where v denotes the drop volume), and denoting the number density by n_λ, we obtain — for large volumes ($\lambda \to 1$) — for the (volume averaged) LWC densities ρ_λ and density squared ρ_λ^2:

$$\begin{aligned} n_\lambda &\to \langle n\rangle \\ \rho_\lambda &\to \langle \rho\rangle \approx \langle n\rangle\langle v\rangle \\ \rho_\lambda^2 &\to \langle \rho^2\rangle \approx \frac{\langle n\rangle\langle v^2\rangle}{\mathrm{vol}S_\lambda} \end{aligned} \tag{4}$$

The central limit theorem then shows that the distribution of the total LWC density converges to a Gaussian probability distribution for the density ρ_λ:

$$\Pr(\rho_\lambda) \propto \exp\left(-\frac{(\rho_\lambda - \langle n\rangle\langle v\rangle)^2 \mathrm{vol}S_\lambda}{2\langle n\rangle(\langle v^2\rangle - \langle v\rangle^2)}\right) \tag{5}$$

Table 1 A comparison of various gauge and radar estimates of α and C_1 over various spatial scales and directions

Data type	Radar reflectivity, Montreal	Gauge, daily accumulations	200 Meteor. Stations, daily accumulations	209 Meteor. Stations (France), daily accumulations[a]	Radar reflectivity, Montreal
Domain	Horizontal space	Horizontal space	Horizontal space	Horizontal space	Vertical space
Range of scales	75 m—19.2 km	150 km to global	5—50 km	30—1000 km	21 m—2.5 km
α	1.4	1.35	1.17—1.54	1.07 ± 0.3	1.35
C_1	0.12	0.16	0.02—0.1	0.35 ± 0.2	0.11
References	Tessier et al. (1993)	Tessier (1993)	Olsson and Niemczynowicz (1996)	Hubert et al. (2002)	Tessier et al. (1993)

The errors are estimated to be about ±0.1 in α and ± 0.05 in C_1.
[a] Private communication.

Table 2 A comparison of various gauge and radar estimates of α and C_1 over various time scales

Data type	Gauge, daily accumulation	Gauge, daily accumulation	Gauge, daily accumulation	Gauge, daily accumulation	Gauge, daily accumulation	Gauge, daily accumulation
Location	Global network	Reunion Island	Nîmes	Germany	New Zealand	Holland, France, Portugal
Sample characteristics	1000 stations 1–64 days	1 station, 30 years, scales 1–64 days	1 station, 30 years, scales 1–64 days	1 station, 45 years, scales 1–32 days	15 s resolution, scales 15 s to 14 h	1 min to 1 month resolution
α	0.5	0.5	0.5	0.6	–	0.48–0.67
C_1	0.6	0.2	0.6	0.5	0.04–0.19	0.30–0.51
References	Tessier et al. (1993)	Hubert et al. (1993)	Ladoy et al. (1993)	Fraedrich and Larnder (1993)[a]	Harris et al. (1996)	De Lima (1998)
Data type	Gauge, 25 stations of daily accumulation	Gauge 164 stations of 6 min and daily accumulations	Radar reflectivity	Radar reflectivity		
Location	Doubs basin (France)	All France	Montreal	Montreal		
Sample characteristics	25 years, scale 1–16 days	4 years, scales 6 h to 16 days	20 m resolution, every 2 s for 5 1/2 h	4 storms, 144 PPIs each 1 km resolution every 5 min		
α	0.62 ± 0.05	0.74 ± 0.15	0.5	0.3–0.6		
C_1	0.38 ± 0.02	0.40 ± 0.1	0.6	0.6–1.2		
References	Hubert et al. (2002)	Hubert et al. (2002)	Tessier et al. (1993)	Seed (1989)		

Note that the C_1 for reflectivities are not expected to be the same as for the gauge rain rates. De Lima (1998) also found that H was systematically of the order of -0.1 (in agreement with Tessier et al., 1996).

[a] Private communication.

i.e., as long as the variance is finite, independent of the drop size distribution, we obtain the ''universal'' Gaussian result for fluctuations in LWC. The continuum limit is obtained by taking $\mathrm{vol}S_\lambda$ large enough that the Gaussian tends to a ''sure'' Dirac delta function: $\Pr(\rho_\lambda) \to \delta(\rho_\lambda - \langle n\rangle\langle v\rangle)$ (i.e., $\rho_\lambda \approx \langle n\rangle\langle v\rangle$).

On the contrary, using the (possibly anisotropic) scale invariance of the system, one expects that the LWC distribution is multifractal and that its probability is scaling according to Eq. (1), i.e. — at resolution $\lambda \gg 1$ — we have for the cumulative probability distribution $\Pr(\rho_\lambda > \lambda^\gamma)$, which is the probability of a random density ρ_λ exceeding a scale dependent threshold λ^γ,

$$\Pr(\rho_\lambda > \lambda^\gamma) \approx \lambda^{-c(\gamma)} \tag{6}$$

As already discussed (''Properties of cascades: conservative multifractals''), this implies a hierarchical clustering of LWC. A multifractal distribution of drops therefore enhances coalescence. As the averaging sphere (diameter $l = L/\lambda$) gets larger ($\lambda \to 1$), the values $\rho_\lambda = \lambda^\gamma\langle\rho\rangle$ do indeed approach their mean $\langle\rho\rangle$; the distribution is less and less ''spread'', but this occurs rather slowly, in a power law way. With smaller and smaller averaging spheres ($\lambda \gg 1$), the fluctuations increase, bringing into sharp relief the role of singularities. While the effect is not so great here, where the outer scale is 2 m, and the mean inter-drop distance is about 10 cm (hence $\lambda = 20$ only), if we consider the global rain process, we may have $L = 10^4$ km (see Lovejoy et al., 2001, and references therein), so that $\lambda = L/r = 10^8$ and the effects of the clustering at all scales can be very large, even for relatively small γ. At the same time, each singularity is distributed over a sparse fractal set of codimensions $c(\gamma)$ as has been directly verified by Lovejoy et al. (1987) on 1 km resolution radar rain data.

Description of the data sets

During the entire three year experiment, the hydrometeors in approximately 450 scenes were photographed. The data sets were all labeled with the reference number of the photographic film used in HYDROP. The digitization of the negatives using the microdensitometer was a time consuming process requiring 30 h per negative (90 h per scene) so that only a few scenes were initially digitized, and only relatively few scenes out of the entire set (18 of 450) have been digitized to date. Out of those, only two different storms (f142 and f207, comprising three realizations each) were analyzed in Desaulniers-Soucy (1999) and each gave very different results (see below) precluding the possibility of drawing any strong general conclusions about the scaling. Since for each storm, the results were quite robust across all three realizations, it was argued that the difference in the results from the different storms could most likely be explained by their very different atmospheric conditions (see Table 3) and corresponding drop size distributions (see Fig. 1). In this paper, we make this interpretation more compelling by considering four additional data sets (f145, f207 comprising the three

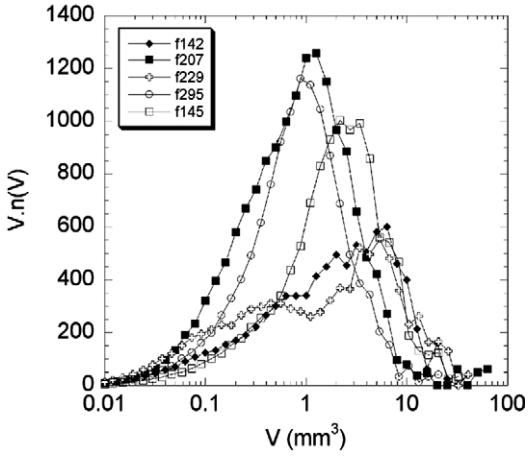

Figure 1 Vn(V) on log-linear scale (areas under the curves are proportional to the total number of drops/volume). For the cumulative distributions, see Fig. 9.

Table 3 The atmospheric conditions were estimated from the McGill University weather station 250 m south of the experiment

Event ID	Date and time	Number of realizations	Volume of ROI (m^3)	Number of rain-drops	Atmospheric conditions	Wind speed at 300 m ($m\ s^{-1}$)	Rain rate ($mm\ h^{-1}$)
f142	November 8th 1996, 7 p.m.	3	8.1	36422/3	Reflectivity bright band at 4 km: melting snow. Rain shower	2.5	2—4
f145	November 8th 1996, 8:30 p.m.	3	8.02	23708/3	Reflectivity bright band: melting snow. Rain shower	22.5	1.4—2.2
f207	July 14th 1997, 12:30 a.m.	7	7.87	59223/7	Convective. Heavy rain.	27.5	6—10
f229	November 1st 1997, 9:45 p.m.	2	7.13	30559/2	Reflectivity bright band at 4 km: melting snow. Embedded convection	17.5	2—4
f295	September 27th 1998, 2:50 a.m.	3	8.04	40100/3	Storm with light precipitation	10	1.4—2.2

This included a UHF vertical sounder which gave both reflectivity profiles and wind speed. Note that for f142, f207, the nominal rain rates estimated from the scenes in Desaulniers-Soucy et al. (2001) were 8—10 mm/h.

initial and four additional triplets, f229 and f295) that were chosen to be representative of various atmospheric conditions and various size distributions. These data sets increased the total number of triplets of photographs analyzed from 6 to 18 and the number of different rain events from two to five.

Table 3 summarizes the salient features of each data set and the atmospheric conditions in which they were obtained. The previously analyzed f142 set, where no scaling was detected, clearly stands out from the others. As shown by a bright band in the McGill University UHF reflectivity profiler radar image, it was of stratiform rain resulting from melting snow at 4 km. Strong coalescence and therefore large rain drops can be expected under these conditions. In addition, winds at 300 m were quite weak so that ground level wind and turbulence were very weak as well. As we discuss below, both these factors lead to weaker small scale coupling of the rain field with the wind field so that we expect the inner scale resulting from the turbulence induced drop clustering to be larger. The f145 data set was obtained 1.5 h later and the strength of the wind at 300 m was about 10 times higher, implying much stronger ground turbulence. The difference in the particle size distribution should also be noted (Fig. 1).

In contrast, f207 was photographed during a convective heavy rain event in the summer period. This event was characterized by: (1) strong winds; (2) high rain rates. The reflectivity profile of f229 indicated a bright band at 4 km but with a zone of embedded convection. The combination of convection and melting snow at 4 km created the conditions for large drop formation. The winds at 300 m were weaker than in f207 or f145 but stronger than in f142.

The f295 data were obtained during a storm with light stratified precipitation in the autumn, explaining the fairly small rain drop sizes. The wind at 300 m, despite being stronger than that of f142, is still weak. Both these factors favor a large inner scale for the coupling of the rain with the wind dynamics. This will be discussed in depth in ''The statistical analysis for increasing scales'' and ''Convergence scale''.

Mention should be made of the representativeness of the meteorological conditions for the cases studied. Each analyzed rain event was chosen without particular regard to the meteorological conditions. They were chosen for practical reasons such as the status of the equipment, the availability of the experimenter, and on the condition that it be night-time rainfall forecasted several hours in advance. As a result of this, the sampling was not biased in any obvious way or systematic manner and should therefore be relatively unbiased with respect to the meteorology.

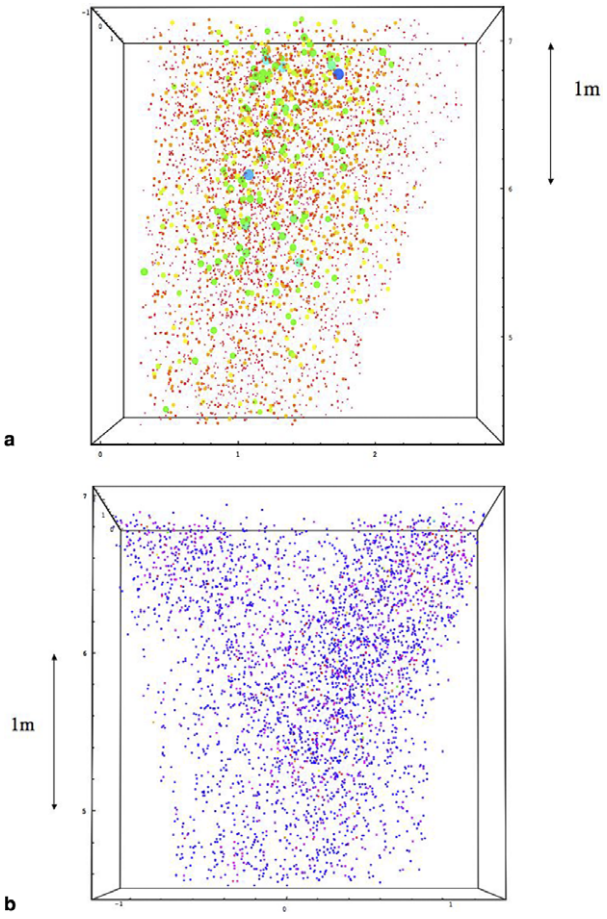

Figure 2 A reconstruction of one of the f295 triplets showing the 15,000 drops in the ROI: only the relative sizes of the drops are accurate. Also displayed is a schematic of the sphere method. The average liquid water content is calculated over NB spheres of radius λ^{-1} randomly centered inside the ROI. The axes *x*, *y* and *z* indicate the width, depth and height of the ROI, respectively. (a) Shows the side view of the largest 10% of the 25,468 drops in one of the f295 scenes. (b) Shows the top view of the same scene but with all the drops. To avoid clutter, the sizes have only been indicated by color (blue small, pink large).

Analysis

The random sphere analysis method

A direct investigation of the large *N* limit can be made by comparing the predictions of the classical continuum with those of the multifractal discontinuum by considering the statistics of rain in spheres of systematically increasing radii *r* (see Fig. 2); this is equivalent to the continuum mechanics thought experiment considered in the introduction. We place gradually larger spheres of radius *r* at random over the ROI and compute the corresponding ''(normalized) η power densities'' at resolution λ (''$\langle\rangle$'' denotes an ensemble average):

$$\rho_\lambda^{(\eta)} \propto \sum_{V_i \in S_\lambda} V_i^\eta; \quad \langle \rho_\lambda^{(\eta)} \rangle = 1 \tag{7}$$

where V_i is the volume of the *i*th drop in the sphere S_λ at scale ratio $\lambda = L/r$, where *L* is the outer scale and *r* the scale of investigation. In Eq. (7), $\rho_\lambda^{(\eta)}$'s are normalized so that the mean is equal to unity. This is a partial correction for the fact that as we change the sphere radius (hence λ), the sample changes slightly due to edge effects discussed below. Note that the rain drops are observed at a much finer resolution $\Lambda \gg \lambda$, where each of them is individualized; $\rho_\lambda^{(\eta)}$ therefore corresponds to a coarse grained observation of the rain drops. Ignoring constants of proportionality, changing η allows us to consider various fields: $\rho_\lambda^{(0)} = n_\lambda$ is the

number density field; $\rho_\lambda^{(1)} = V_\lambda$ is the LWC, $\rho_\lambda^{(1/3)} = d_\lambda$ is the rain-drop diameter field, $\rho_\lambda^{(7/6)} = R_\lambda$ is the nominal rain rate (assuming a terminal fall speed proportional to the square root of the drop radius[4]), and $\rho_\lambda^{(2)} = Z_\lambda$ is the radar reflectivity factor field. Following Eq. (2), for each η we can define a moment scaling exponent $K(q,\eta)$:

$$\langle(\rho_\lambda^{(\eta)})^q\rangle \propto \lambda^{K(q,\eta)} \tag{8}$$

At each scale λ and for each moment q, the ensemble averaging was approximated by an average over 5000 spheres, with centers uniformly randomly distributed within the ROI, and over the total number of available data sets for a given precipitation event. The 5000 spheres were partially overlapping and as such were not independent. While there is no reason to expect the non-independence of the spheres to lead to a bias in the multifractal results, it will affect the theoretical error in parameter estimates.

Since the centers of the spheres are generated uniformly anywhere inside the ROI, some spheres — especially the larger ones of size of the order of the dimensions of the ROI — may extend partially outside the ROI. Instead of discriminating against all spheres extending outside the ROI (which would greatly reduce the statistics for the larger scales), it was decided to consider all spheres whose centers were inside the ROI and whose volume was >50% inside the ROI, and compensate for the fraction extending outside by assuming the inside and outside densities to be equal (see Desaulniers-Soucy, 1999). So as to avoid unacceptable biases, spheres whose volume was >50% outside the ROI were thus rejected from the analysis. This procedure has the disadvantage that the extrapolation of a sphere's statistics inside the ROI to outside the ROI effectively amounts to making a relatively minor homogeneity assumption, i.e. the variability at larger scales is slightly reduced by this technique. This is of course true only for a small fraction of the spheres and a small fraction of the volume of the ROI. However, in keeping with the objective of maximizing the statistics and the range of scales, this approach was favored over the stricter discriminative one of rejecting any sphere extending at the outside of the ROI. At the same time, since a gradually larger fraction of the spheres extends outside the ROI as r is increased, the sample under investigation changes somewhat with scale (the larger spheres have a tendency to have their centers closer to the middle of the ROI; those with centers far from the middle of the ROI are more likely to extend outside the region by >50% and be rejected from analysis). This is partially corrected by the fact that we are considering normalized powers (see Eq. (7)) at all resolutions λ. This also partially removes small residual biases coming from the inhomogeneities in the estimate of the illumination field. The sphere method has the added advantage (over other box counting type methods) of maximizing the use of the ROI, since the latter is a three dimensional trapezoid bounded by the combined field of view of the HYDROP set-up and the region uniformly illuminated by the flash lamps (see Desaulniers-Soucy, 1999; Desaulniers-Soucy et al., 2001). In the figures below (''The statistical analysis for increaing scales''), we computed the statistical moments $\langle(\rho_\lambda^{(\eta)})^q\rangle$ over spherical regions of logarithmically increasing size ratio $\lambda = R/r$ where r is bounded above by the size of the largest allowable sphere of radius R ($2m$) and below by the experimentally accessible inter-particle distance (typically of the order of 10 cm). The maximum range of scales is therefore $\lambda \approx 20$, but spheres of radii <10 cm contained on average so few particles that we only display statistics over a range of factor 10.

[4] The square root law is commonly used as the fall speed in the high Reynolds number regime although the $d^{2/3}$ fall speed may be more accurate (Atlas and Ulbrich, 1977); this would imply $\rho_\lambda^{(11/9)} = R_\lambda$.

The statistical analysis for increasing scales

Figs. 3–7 show $\log_{10}\langle(\rho_\lambda^{(\eta)})^q\rangle$ as a function of $\log_{10}(\lambda)$ with $\eta = 0$ (a), $\eta = 1/3$ (b) and $\eta = 1$ (c), for the f145, f207, f229, f295 and f142, respectively, as computed by Eq. (7) and as detailed in ''The random sphere analysis method''. The nominal rain rate exponent $\eta = 7/6$ is close enough to the case $\eta = 1$ that we do not repeat the analysis for the value 7/6 (in any event, to compute true rain rate, we would need the fall speed of each rain-drop). The $\eta = 2$ case (corresponding to the radar reflectivity factor Z) is discussed in section 4.6. The $\eta = 0$ results, which are not affected by the drop sizes but only the locations, and which will therefore be expected to converge at scales smaller than for the corresponding $\eta > 0$ scales are strongly curved for a large enough λ (small enough r and N). With the exception of f142 however, they appear to approach straight lines at large enough scales as predicted by the scaling. The ''spread'' of the moment values at the largest scales ($\log\lambda = 0$) is purely due to the difference in the spatial means between the different scenes comprising each storm ensemble; for a given η, we can compare the moments for different storms; this shows which ensemble had the smallest scene-to-scene variability. For larger η, we see the same basic behavior except that the onset of the linearity is at somewhat larger scales.

Given the admittedly small range of scales over which the scaling is observed, it is important to check that the observed behavior could not arise from the standard large N limit simply as a classical statistical fluctuation. It is straightforward to check this by comparing the observed statistical moments with the classical predictions by retaining the measured drop sizes but by randomizing their positions and then analyze again as before. Within the limits of small statistical fluctuations (which themselves were checked by repeating the randomization and checking the robustness of the result), all differences between the randomized data sets and the real ones are due solely to the long range correlations in the drop positions. These randomized curves are directly superposed in Figs. 3–7; they show — with the exception of f142 — a significant systematic increase at all scales in the variability of the real data with respect to the randomized data. Furthermore, as expected, since for large N, they approach a Gaussian distribution — on these log–log plots, all moments are curved asymptotically approaching a flat line at large enough N, the (nonzero slope) linearity of the real data is in strong contrast.

It should be noted that the randomized statistics can also be used as the basis of rigorous statistical hypothesis testing; specifically, we performed χ^2 tests to test the statisti-

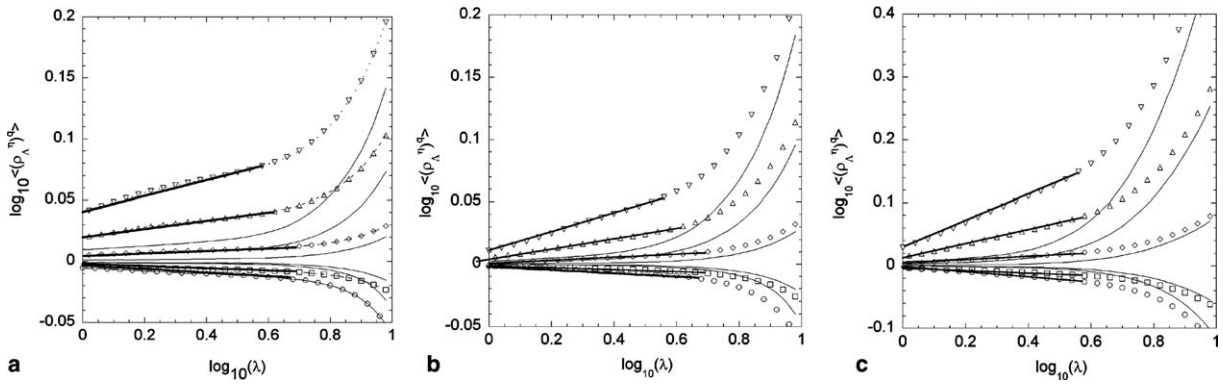

Figure 3 Statistical moments of order $q = 0.4, 0.8, 1.2, 1.6, 2.0$ for f145 (bottom to top). (a) $\eta = 0$. (b) $\eta = 1/3$. (c) $\eta = 1$. As the order q is increased, the statistical moment increases in slope and in amplitude. The solid lines are the statistical moments calculated for the randomized drop positions, the data points are the statistical moments calculated for the real drop positions. The straight solid lines identify the regions over which scaling is observed. For fixed η, increasing the statistical order q emphasizes the rare but large fluctuations — spheres with particularly large N for $\eta = 0$, and spheres with particularly large LWC for $\eta = 1$ (the particle size distribution becomes important) — they require more rain-drops (smaller λ) to converge. Small values of q emphasize the more common small fluctuations. For both large η and q, we expect convergence problems to become more and more severe.

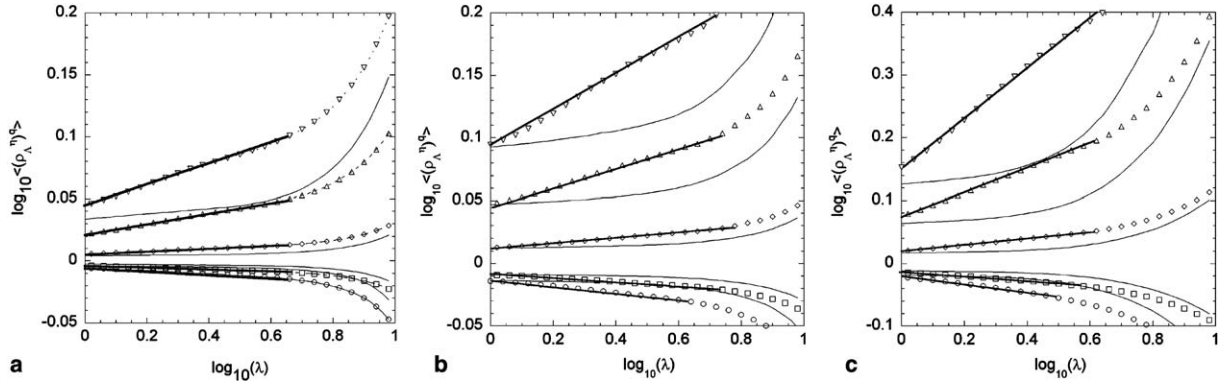

Figure 4 Same as Fig. 3 but for f207.

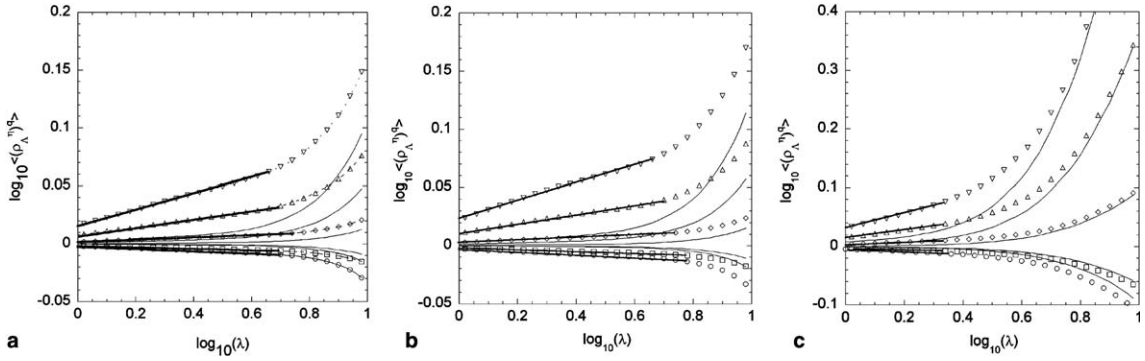

Figure 5 Same as Fig. 3 but for f229.

cal hypothesis that the data were indeed taken from a spatially homogeneous drop distribution. Although the results depend on scale and on the exact data set, the hypothesis of a homogeneous population could typically be rejected with great certainty (at confidence levels of 0.9999 or greater).

Contrary to the homogeneous classical limit, multiscaling of the statistical moments of the η-densities agrees with the experimental results of Figs. 3—6. The statistics depend strongly on the averaging volume in a power law manner. The one exception is Fig. 7, f142, for which the real data have not converged to multifractal statistics

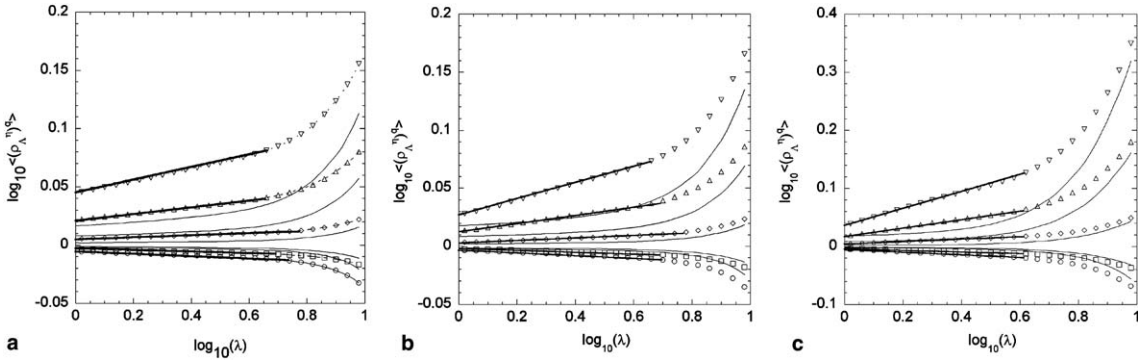

Figure 6 Same as Fig. 3 but for f295.

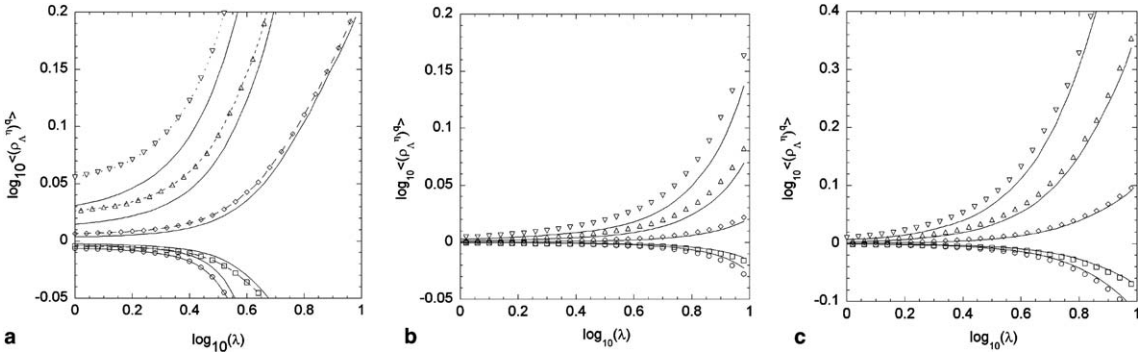

Figure 7 Same as Fig. 3 but for f142.

and which are close to the moments of the randomized coordinates. This case has weak winds (Table 3) and largest drops (Table 4), a combination which is expected to lead to a larger scale of convergence which was not reached given the accessible range of scales in HYDROP; we make this case more strongly below (''Convergence scale''). (Note added at press time: energy spectra of the drops (considered as a multifractal measure i.e. a set with a ''weight'' given by the drop volume) gives not only additional confirmation of the scaling, but shows that the latter is quite close to the Corrsin-Obukhov result predicted for a passive tracer (i.e. the energy spectrum $E(k) \approx k^{-\beta}$, $\beta = 5/3$, wavenumber k). At the high wavenumbers, on the contrary, the spectra are those of a white noise (also) as expected; the transition scale being roughly the same as those determined with the sphere method).

Convergence scale

Identifying significant scaling requires both a wide range of scales and also — because of the large fluctuations in drop size — sufficiently large N. However, the data will presumably only be multiscaling if the rain is coupled to atmospheric fields. At the very least, the coupling of the rain to the dynamics depends on the strength of the turbulence and on the rain-drop size: at small enough scales, drop inertia could destroy the induced hierarchical clustering. This effect is particularly important for the heavier drops which, due to their larger inertia, decouple more easily

Table 4 Comparisons of the scale of convergence r_c to the multifractal large N limit, estimated from Figs. 3–7 for $\eta = 1$, $q = 2$, and of the corresponding average number of drops per sphere of radius r_c

Event ID	Scale of convergence r_c for $\eta = 1$, $q = 2$ (cm)	N_c = average number of drops per sphere at r_c	$\eta = 1$ critical volume (mm^3)	$N_{d,1}$ = number of drops for $\eta = 1$ convergence	$\eta = 2$ critical volume (mm^3)	$N_{d,2}$ = number of drops for $\eta = 2$ convergence
f142	—	—	1.7	33	7.0	165
f145	24	57	1.5	7	3.8	33
f207	20	36	0.75	13	3.0	111
f229	40	574	3.0	80	10.0	625
f295	23	96	0.5	5	1.5	20

For comparison, we also show the expected number of drops for $\eta = 1$ and $\eta = 2$ convergence purely from the drop size distribution.

than smaller ones. The scale of convergence to the multifractal limit will therefore depend on the rain-drop size distribution and the intensity of the turbulence. In the simplest model, the scale of convergence depends only on these two factors. From a theoretical point of view, this can be understood quite simply in terms of the usual — although not so realistic — assumption that the drop fall speed $v_f(\delta)$ is determined by the diameter δ only (e.g., it falls at the still air terminal velocity, the past history is irrelevant). In this case, by equating $v_f(\delta)$ to a typical shear Δv across a region of size Δx expressed using Kolmogorov scaling as $\Delta v = \varepsilon^{1/3}\Delta x^{1/3}$ (recall ε is the energy flux characterizing the intensity of the turbulence), we obtain an estimate of the drop size and shear strength decoupling scale $\Delta x = r_c$:

$$r_c = \frac{v_f(\delta)^3}{\varepsilon} \tag{9a}$$

If we further assume that $v_f(\delta) \propto \delta^{1/2}$ (which is a classical result obtained by using the terminal fall speed in the high Reynolds number/large drop limit), then we find the decoupling scale:

$$r_c \propto \frac{\delta^{3/2}}{\varepsilon} \tag{9b}$$

Eq. (9b) displays the realistic dependence of the inner scale of convergence on meteorological conditions via the level of turbulence and on drop inertia. Keeping this simple picture in mind, we can use the meteorological data presented in ''Description of the data sets'' combined with the measured drop size distributions to demonstrate the consistency of our results for each storm, i.e., that it can indeed explain the observed storm to storm variations in inner scales consistently with Eqs. (9a) and (9b).

From the scale at which linear (scaling) behavior is observed, we can now use Figs. 3—7 to directly estimate the inner scale r_c and its corresponding average number of drops N_c in a sphere of radius r_c. Table 4 gives the inner scale of convergence r_c estimated in this way from Figs. 3—7. These r_c and N_c estimates can then be compared to those expected purely on the basis of the drop size distribution r_d and N_d (i.e., without taking into account any drop position correlations). Since we suggest in this paper that the inner scale of convergence depends on the coupling between the turbulent velocity field and the rain-drops, by classifying the five data sets according to the average drop size and the wind velocity, we can at least qualitatively place them in order of increasing convergence scale (see Fig. 8). This serves as a consistency check and an interpretation of the r_c's evaluated quantitatively (see Table 4).

In order to estimate r_d and N_d, consider the rain drop size distributions re-plotted on a cumulative log—log plot in Fig. 9. The advantage of these plots is that they give direct information about the scale of convergence of statistical moments of various orders. Indeed, if the maximum of the probability distribution $\Pr(V \geqslant v) = e^{-c(\log v)}$ is sufficiently ''peaked'', the maximum contribution to the ηth statistical moment comes from rain-drops of volumes corresponding to $\eta = c'$, where c' is the logarithmic derivative of the probability distribution (see, e.g. Desaulniers-Soucy, 1999; Desaulniers-Soucy et al., 2001). For independent drops, the main contributors to the mean, $\eta = 1$, and variance, $\eta = 2$ (they are fundamental for the central limit theorem convergence to the classical large N limit), are raindrops of size corresponding to the tangent of slopes -1 and -2, respectively, to the exceedance probability histogram $\log(\Pr(V \geqslant v))$ versus $\log V$. To estimate r_d, we use the second order moment since it is the critical moment for standard central limit convergence and find V_d graphi-

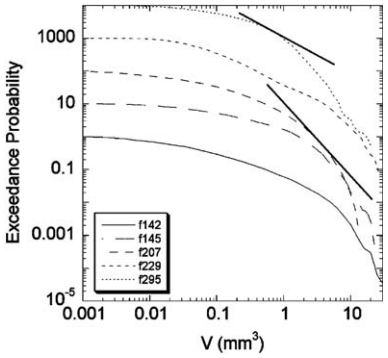

Figure 9 Exceedance probability histogram for all five events. Each curve has been shifted up by one order of magnitude more than its neighbors below for clarity. The reference lines have slopes of 1, 2 indicating the critical volumes and probabilities for the first and second order moments.

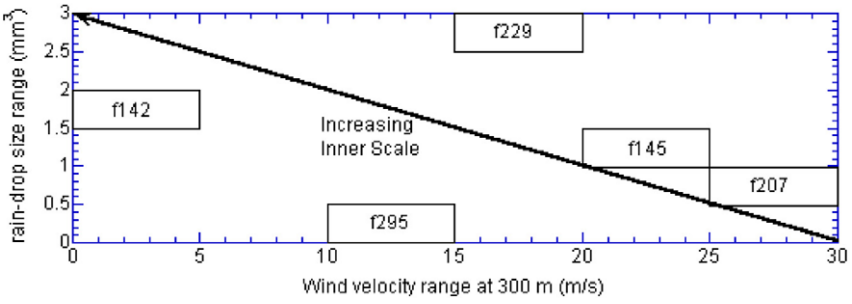

Figure 8 This figure depicts the dependence of the inner scale of convergence on both the dominant particle size and the turbulence. The smallest inner scale (f207) is achieved in conditions of high winds combined with small particle sizes. The largest inner scale — f142, for which the inner scale of convergence was outside our experimentally attained range of scales — is obtained for weak winds and large raindrops. All other cases are intermediate, see ''The statistical analysis for increasing scales''.

cally as the point where $d\log(\Pr(V \geqslant v))/dV \approx -2$. From V_d, we obtain r_d and the number of independent drops needed for convergence of the corresponding moments is $N_d \approx \Pr(V \geqslant v)^{-1}$. The difference between N_d and N_c is thus purely due to the spatial correlations present in N_c but absent in N_d.

As an example, in f142, drops with volumes exceeding 1.7 mm^3 are the dominant contribution to the mean but represent only 3% of the drops in the ROI. The dominant contribution to the variance is determined in the same way, by drawing the tangent of slope -2 to the exceedance probability histogram. In f142, drops larger than 7 mm^3 are the dominant contribution to the variance but represent only 0.61% of the drops in the ROI; the corresponding N_d are the reciprocal of the probabilities and are rough estimates of the number of drops necessary for convergence of the corresponding moments if inter-drop correlations are neglected.

By comparing N_c with $N_{d,1}$ and $N_{d,2}$, in Table 4, we see that they tend to vary in the same direction. However, the fact that these numbers do not vary in the same ratio (for example, although N_c varies by a factor of 20, $N_{d,2}$ by a factor of 30 and the ratio $N_c/N_{d,2}$ varies by a factor of 15) indicates that the variations in drop size only partially account for the variations in N_c. These results and observations highlight the fact that it is the coupling to the dynamics — which depends both on particle size distribution and turbulence intensity — that appears to determine the scale of convergence to the multifractal limit.

Number, volume and (normalized) ηth power density drop size distributions and (mono) fractal drop distributions

In the classical approach to precipitation, the hydrometeor number size distribution plays a fundamental role, hence the perennial debate on exponential versus lognormal versus Weibull (or other) drop size distributions (e.g., Kostinski and Jameson, 1999). In contrast, in the scale- invariant regime of a multifractal rainfield (i.e., in spheres containing large numbers of drops), it is the η-densities (n, V, Z, etc.) which have relatively straightforward universal behavior; neither the drop size distribution nor the spatial distribution of individual drops need be universal and hence be amenable to meaningful (robust) parameterization. Physically, these densities are rather determined by the large scale turbulent fluxes (water, energy etc.). Nevertheless, the influence of the drop size distribution can be gauged by considering the (normalized) ηth power densities: by varying the value of η to which the drop volumes are raised, we obtain fields which are increasingly sensitive to the larger drops in the distribution.

Let us consider briefly the number density which has already been the subject of several fractal correlation dimension analyses mentioned earlier. The statistics of n_λ can be related to box codimensions C_s (the dimension of the support of the rain) and the ''correlation codimension'' C_c by: $C_s = -K_n(0)$, $C_c = K_n(2)$. Recall that the number of boxes of size λ^{-1} needed to cover a set $\propto \lambda^{D_s}$ with $D_s = d - C_s$ = *box dimension*. Similarly, the number of pairs of drops within a distance λ^{-1} varies as λ^{-D_c} with $D_c = d - C_c$ = *correlation dimension*. We could also note that sometimes the information dimension $D_I = d - C_I$ is of interest; here $C_I = K'(1) = C_1$. From Table 5, using the values of C_1 and α we find $C_c = K_n(2) \approx 0.07 \pm 0.02$. Before comparing it with the value 0.17 found by Lovejoy and Schertzer (1990) for the blotting paper (or the value 0.07 found by Zawadski (1995) for small drops in disdrometer time series), we should make two comments. The first is that the universal fits have been made assuming that rain is space filling, i.e., $C_s = -K_s(0) = 0$. Although $K_s(0) = 0$ was indeed close to the data, the experiment was conditioned on the existence of rain so that a small non-zero D_s could not be excluded simply on the basis of the measurements reported here. The second point is that the present results show the importance of considering scaling at scales above the inner decoupling scale r_c. Although r_c is a function of meteorological conditions, it is apparently often 30 cm or more. This means that in the correlation dimension analyses, we should first attempt to estimate this decoupling scale, and then the scaling at larger scales. Such a refined analysis was not possible with the 452 drops studied in the single realization discussed in Lovejoy and Schertzer (1990) but is possible in the present study which is based on far larger numbers of drops.

Universal multifractal parameters

For the four rain events for which the large N data converge to a scaling limit (i.e., with the exception of f142), using non-linear regression, we fit the observed $K(q)$'s (the slopes in linear regimes in Figs. 3–6) to the universal form (Eq. (3)), and estimated the multifractal parameters α and C_1. Table 5 summarizes the results. The non-linear fits were performed for $0 < q < 1.5$ and are shown in Fig. 10. The reason for the restriction to low q is that the universal form, Eq. (3), is only valid up to the critical moment order q_s (''Properties of cascades: conservative multifractals''). After q_s, $K(q)$ becomes straight: the slope is equal to the largest singularity present in the sample. In the case of $\eta = 1$, we found $\alpha = 1.5 \pm 0.2$ and

Table 5 Summary of the multifractal parameters estimated from the moment scaling function $K(q)$ for the four storms with inner scale <1 m

Event ID	$\eta = 0$ C_1	$\eta = 0$ α	$\eta = 1/3$ C_1	$\eta = 1/3$ α	$\eta = 1$ C_1	$\eta = 1$ α
f145	0.039	1.4	0.044	1.5	0.13	1.6
f207	0.046	1.7	0.090	1.4	0.24	1.3
f229	0.037	1.6	0.042	1.7	0.10	1.6
f295	0.032	1.6	0.040	1.6	0.09	1.6

$\eta = 0$, 1/3, 1 corresponds to n, d and V, respectively.

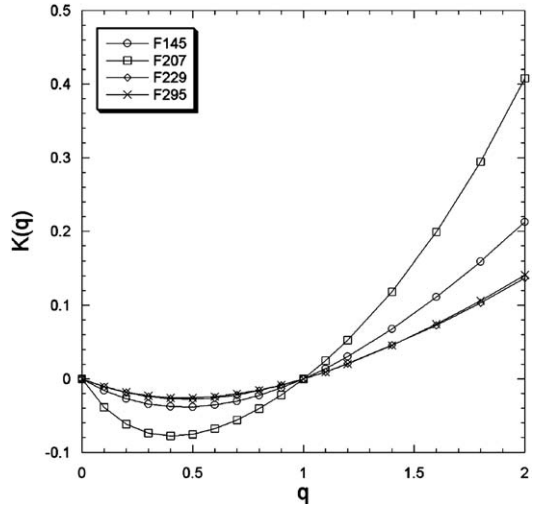

Figure 10 Universal multifractal $K(q)$ vs. q for f145, f207, f229 and f295 for $\eta = 1$. The lines are the regressions using the parameters indicated in Table 5.

$C_1 = 0.14 \pm 0.06$ by taking the mean of the estimates in Table 5. These results are comparable to the values found at larger scales for both rain (see Tables 1 and 2) and in turbulence (e.g., $\alpha = 1.5$, $C_1 = 0.08$ for the wind field, Schmitt et al., 1992). We obtain very similar results for α for all data sets and all values of η studied. Furthermore, $\alpha_n = \alpha_1 = \alpha = const.$ was directly confirmed by taking regressions of $\log\langle(\rho^{\eta_1})^q_\lambda\rangle$ against $\log\langle(\rho^{\eta_2})^q_\lambda\rangle$ for various η_1, η_2 which were found to be fairly linear with slopes equal to $(\eta_1/\eta_2)^\alpha$ independent of q. These tests indicated that the α is independent of η, with a value of about 1.5.

Up until now, we have not discussed the non-conservation parameter H. The most convenient way to measure H is via spectra; the result (work in progress) mentioned earlier that the low wavenumber spectral exponent was close to the passive scalar value $\beta \approx 5/3$ implies $H \approx 1/3$.

At first sight, the value of C_1 may seem small. For example, it implies that if we consider an experiment in the scaling regime with $C_1 = 0.14$ (our average for LWC, i.e., $\eta = 1$) over a range of scales $\lambda = 10$ (somewhat larger than the scaling regime here), then the fraction of the volume which contributes substantially to the mean is $\lambda^{-C_1} = 72\%$ which is not much below the continuum result (100%). Even if we consider the second moment, we find from the Legendre transform (Eq. (2b)) that the dominant singularity is $\gamma = K'(2) = 0.31$ (using $\alpha = 1.5$), and the corresponding contributing fraction $\lambda^{-C(0.31)} = 40\%$. It would not be surprising to find that with the use of several carefully selected parameters, classical (i.e., non-scaling) compound Poisson processes A could be arranged so as to reproduce this relatively mild inhomogeneity. It is only if we start to consider the large ranges of meteorologically significant scales that the difference between the large N multifractal and continuum limits becomes important. For example, even if the multifractality only holds up to the scale of a typical weather radar pulse (1 km^3 say, i.e., $\lambda = 10^3/10^{-1} = 10^4$), then the corresponding figures are 28%, 2.6% for the mean and variance: the classical compound Poisson would require a drastic change in ''optimum'' parameters in order to even approximate this level of heterogeneity; indeed, it would probably already demand that the Poisson parameters themselves vary in a scaling way; the ''multifractal compound Poisson process'' to be discussed in a forthcoming publication. The situation is likely to be even more drastic since — as the largest study of atmospheric statistics to date shows (nearly 1000 satellite photographs in Lovejoy and Schertzer, 2006; Lovejoy et al., 2001) — the outer scale is of the order of 10^4 km, then $\lambda = 10^8$ which yields, respectively, 8%, 0.07% of the volume.

Implications of universality for the radar reflectivity factors Z ($\eta = 2$)

Since we have no velocity information for the individual drops, we cannot properly estimate R, and we cannot directly verify the statistical ZR relation. However, we can attempt to test the analogous ZV relation (i.e., the above for $\eta = 2$ and $\eta = 1$). The only difficulty is that $\eta = 2$ corresponds to a fairly high order moment. Depending on the inner scale for a given storm, scaling may not be obtained over a sufficiently wide range in order to be clearly visible. Considering the case with the smallest inner scale (widest scaling range) f295, Fig. 11 shows the resulting scaling with some evidence for convergence at the largest accessible scales. By fitting the universal form of $K(q)$ to the slopes of the moments, we obtain an estimate $C_{1,Z} \approx 0.21$ and $\alpha \approx 1.5$, which are reasonably close to the values found for the effective radar reflectivity factor in radar data in Tessier et al., 1993: $C_{1,Ze} \approx 0.12$ and $\alpha \approx 1.4$.

When comparing our exponents with real radar values, we can already note that radars do not measure Z, but rather the ''effective Z'' (Z_{eff}) which differs from Z because of the modulation by position and radar wave-vector dependent phase factors. In contrast, Z is a primarily theoretical quantity requiring HYDROP type 3-D data for its determination. In the classical large N limit, the drop positions are statistically independent, hence the drops scatter

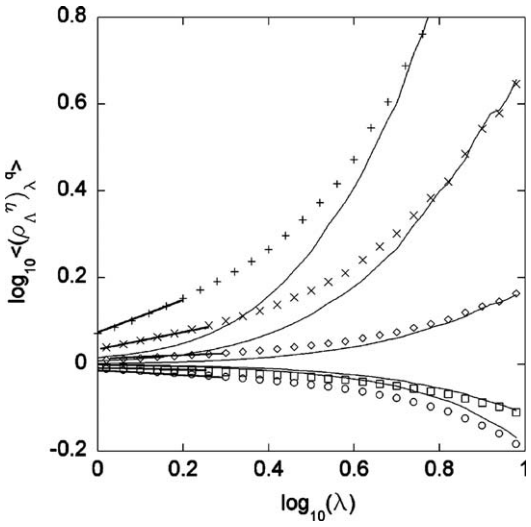

Figure 11 Statistical moments of order $q = 0.4$, 0.8, 1.2, 1.6, 2.0 for f295 for $\eta = 2$, corresponding to the radar reflectivity Z. The solid lines are the statistical moments calculated for the randomized drop positions, the data points are the statistical moments calculated for the real drop positions.

incoherently; however, in the multifractal large N limit, the clustering at all scales implies some degree of coherent scattering so that there is a systematic scale dependent bias if Z_{eff} is used as a surrogate for Z (see Lovejoy et al. (1996) for a full analysis of this ''multifractal observers problem'').

Conclusion

A central concept in atmospheric physics is the particle size distribution $N(\delta)$, the number of particles per unit volume with diameter between δ and $\delta + d\delta$. Although it is rarely stated explicitly, $N(\delta)$ is only well defined if the large particle number (N) limit is the classical continuum. Specifically, if $N(\delta)$ is defined on a sphere of radius r, there should exist a range of scales over which $N(\delta)$ is independent of r. Based on stereophotography of rain drops in a roughly 8 m^3 volume, we directly examined the statistics as a function of r (equivalently of N), finding that, in at least four of the five storms studied, the large N statistics are close to power laws; the statistics are multifractal in contradiction with the classical continuum. Since the turbulence is multifractal, this is a natural consequence of the dynamical interaction between the turbulence and the particles. Due to complex inter-drop processes, we do not expect the wind and precipitation to have the same statistics, however, these interactions need not break the scaling and, apparently, only modify the exponents α and C_1 a little if at all. Similarly, we find that in the observed large N scaling regime, the exponent parameters α and C_1 values are not far from other estimates in rain at much larger scales. In the multifractal limit, although the statistics are continuous, each realization is singular with respect to the usual Lebesgue measures; hence in this sense, the large N limit is a ''discontinuum''. According to this, the main difference between the rain rate and wind statistics is the non-conservation parameter H which, for the horizontal wind as a function of horizontal displacement, has the Kolmogorov $H = 1/3$ value whereas for the rain rate, H is apparently close to zero (although as mentioned above, the LWC statistics do have $H \approx 1/3$).

According to this picture, the fields of meteorological interest (drop number n, LWC, V, rain rate R, radar reflectivity Z, etc.) are controlled by turbulent processes acting over a wide range of scales; these determine the fundamental scaling exponents. However at small enough scales, we identified a direct role for the drop size distributions in determining the inner scale which we argued is roughly proportional to $\delta^{3/2}$ while inversely proportional to the intensity (ε) of the turbulence (Eq. (9b)). This was supported by a comparison with the single storm (f142) for which no inner scale was observed; it had both very large drops and very small ε (inferred by UHF radar wind measurements). Quantitative analysis of the observed inner scales in the four other cases supported this simple picture. By comparing the rains of the different storms, we gave direct empirical evidence in favor of this picture.

By fitting the observed scaling exponent functions into multifractal universality classes characterized by the two fundamental exponents α and C_1, we showed that the highly variable fields were quantitatively compatible with the turbulent coupling. This is in qualitative agreement with the multiplicative phenomenology and lognormal parametrization of rain. However, quantitatively, the value of $\alpha \approx 1.5$ is already different from the lognormal value $\alpha = 2$. We also remarked that, in any case, the probability tails (of n, V, R, Z, but not necessarily of the drop sizes) are likely to be algebraic (power law). Insofar as the universal multifractal picture is valid, the exponents coupled with the inner scale then allow us to calculate all the LWC statistics at all scales. More direct evidence for turbulent coupling comes from spectral analysis (work in progress) which shows a transition from large scale (>30–50 cm) passive scalar spectra to small scale white noise spectra.

If these findings are supported by others – preferably at somewhat larger scales perhaps along the lines of work in progress by Cârsteanu and Castro (2002) – then the emphasis of precipitation physics will no longer be on precipitation characteristics at fixed scales/resolutions, but rather in the exponents which allow us to calculate the statistics at any scale/resolution over the scaling regime. At the same time, the scale dependent relations which emerge are not deterministic, but rather statistical so that a stochastic formulation (and corresponding multifractal modeling) will be necessary. Since longstanding problems in precipitation physics hinge on comparing fields at different space–time resolutions (e.g., rain gauge versus radar reflectivities), the emerging scaling relationships between different precipitation fields are promising.

Acknowledgements

We are very grateful to Mr. Peter B. Stetson of the Dominion Astrophysical Observatory in Victoria for the digitization of the photographic negatives. We are also grateful to Mr. Robert Nowak for relentless support at various stages of this study. The financial assistance from the Faculty of Graduate Studies and Research, the Meteorological Service of Canada, the National Science and Engineering Research Council and the Fonds pour la formation des chercheurs et d'aide à la recherche was greatly appreciated. D. Schertzer acknowledges fruitful discussions with J.L. Brenguier (Meteo-France, Centre National de Rechereches Météorologiques) and D. Lhuillier (Laboratoire de Modélisation, Université Pierre et Marie Curie), as well as partial support from PNRH and RIO programs. S. Lovejoy and M. Lilley acknowledge the hospitality of the Laboratoire de Modélisation en Mécanique in the fall of 2002 and winter of 2003, which made collaboration with D. Schertzer possible in the final stages of this work.

References

Anselmet, F., Antonia, R.A., Danaila, L., 2001. Turbulent flows and intermittency in laboratory experiments. Planet. Space Sci. 49, 1177–1191.

Atlas, D., Ulbrich, C.W., 1977. Path- and area-integrated rainfall measurement by microwave attenuation in the 1–3 cm band. J. Appl. Meteor. 16, 1322–1331.

Batchelor, G.K., 1970. An Introduction to Fluid Mechanics. Cambridge University Press.

Beard, K.V., 1976. Terminal velocity and shape of cloud and precipitation drops aloft. J. Atmos. Sci. 33, 851–864.

Bendjouhdi, H., Hubert, P., Schertzer, D., Lovejoy, S., 1997. Multifractal point of view on rainfall intensity–duration–fre-

quency curves. C.R.Acad. Sci. Paris, Série II, Fasc. A 325 (5), 323–326.
Brenguier, J-.L., 1993. Observations of cloud microstructures at the centimeter scale. J. Appl. Meteorol. 32, 783–793.
Cârsteanu, A., Castro, J., 2002 EGS presentation, Nice 2002.
Cârsteanu, A., Foufoula-Georgiou, E., 1996. Assessing dependence among weights in a multiplicative cascade model of temporal rainfall. J. Geophys. Res. 101 (D21), 26363–26370.
Davis, A., Marshak, A., Wiscombe, W., Cahalan, R., 1996. Scale invariance of liquid water in marine stratocumulus. Part I: spectral properties and stationary issues. J. Atmos. Sci. 53, 1538–1560.
De Lima, I., 1998. Multifractals and the temporal structure of rainfall, Ph.D. thesis, Wageningen University, The Netherlands.
Desaulniers-Soucy, N., 1999. Empirical test of the multifractal continuum in rain, Ph.D. thesis, McGill University, Montréal.
Desaulniers-Soucy, N., Lovejoy, S., Schertzer, D., 2001. The HYDROP experiment: an empirical method for the determination of the continuum limit in rain. Atmos. Res. 59–60, 163–197.
Fabry, F., 1996. On the determination of scale ranges for precipitation fields. J. Geophys. Res. D101, 12819–12826.
Fraedrich, K., Larnder, C., 1993. Scaling regimes of composite rainfall time series. Tellus 45A, 289–298.
Frisch, U., Sulem, P.L., Nelkin, M., 1978. A simple dynamical model of intermittency in fully developed turbulence. J. Fluid Mech. 87, 719–724.
Gabella, M., Pavone, S., Perona, G., 2001. Errors in the estimate of the fractal correlation dimension of raindrop spatial distribution. J. Appl. Meteor. 40, 664–668.
Gupta, V.J., Waymire, E., 1990. Multiscaling properties of spatial rainfall and river flow distributions. J. Geophys. Res. 95, 1999–2010.
Gupta, V.J., Waymire, E., 1993. A statistical analysis of mesoscale rainfall as a random cascade. J. Appl. Meteorol. 32, 251–267.
Harris, D., Foufoula, E., Droegemeir, K.K., Levit, J.J., 2001. Multiscale statistical properties of a high-resolution precipitation forecast. J. Hydrometeor. 2, 406–418.
Harris, D., Menabde, M., Seed, A., Austin, G., 1996. Multifractal characterization of rain fields with a strong orographic influence. J. Geophys. Res. 101, 26405–26414.
Hubert, P., 1995. Fractals et multifractals appliqués à l'étude de la variabilité temporelle des précipitations. In: Feddes, R.A. (Ed.), Space and Time Scale Variability and Interdependencies in Hydrological Processes. Cambridge University Press, UK, pp. 175–181.
Hubert, P., Carbonnel, J.-P., 1989. Dimensions fractales de l'occurrence de pluie en climat soudano-sahélien. Hydrologie Continental 4 (1), 3–10.
Hubert, P., Tessier, Y., Ladoy, P., Lovejoy, S., Schertzer, D., Carbonnel, J.P., Violette, S., Desurosne, I., Schmitt, F., 1993. Multifractals and extreme rainfall events. Geophys. Res. Lett. 20, 931–934.
Hubert, P., Biaou, A., Schertzer, D., 2002. De la Méso-Echelle à la Micro-Echelle: Désagrégation/Agrégation Multifractale et Spatio-Temporelle des Précipitations. Report, Armines-EdF.
Jameson, A.R., Kostinski, A.B., 1998. Fluctuation properties of precipitation: Part II. Reconsideration of\the meaning and measurement of raindrop size distributions. J. Atmos. Sci. 55, 283–294.
Jameson, A.R., Kostinski, A.B., 1999. Fluctuation properties of precipitation: Part V: Distirbution of rain rates — theory and observations in clustered rain. J. Atmos. Sci. 56, 3920–3932.
Jameson, A.R., Kostinski, A.B., 2000a. Fluctuation properties of precipitation part VI: observation of hyperfine clustering and drop size distribution structures in three dimensional rain. J. Atmos. Sci. 57, 373–388.
Jameson, A.R., Kostinski, A.B., 2000b. What is a raindrop size distribution? Am. Meteorol. Soc. 82, 1169–1177.
Jameson, A.R., Kostinski, A.B., 2001. Comments on ''Errors in the estimate of the fractal correlation dimension of raindrop spectra distribution''. J. Appl. Meteor. 40, 2098.
Jameson, A.R., Kostinski, A.B., 2002. Spurious power-law relations among rainfall and radar parameters. Q.J.R. Meteor. Soc. 128, 1–14.
Jameson, A.R., Kostinski, A.B., Kruger, A., 1999. Fluctuation properties of precipitation: Part IV. Fine scale clustering of drops in variable rain. J. Atmos. Sci. 59, 82–91.
Kostinski, A.B., Jameson, A.R., 1997. Fluctuation properties of precipitation: Part I. On deviations of single-size drop counts from the Poisson distribution. J. Atmos. Sci. 54, 2174–2186.
Kostinski, A.B., Jameson, A.R., 1999. Fluctuations properties of precipitation part III: on the ubiquity and emergence of exponential drop size distributions. J. Atmos. Sci. 56, 111–121.
Kozikowska, A., Haman, K., Supronowicz, J., 1984. Preliminary results of an investigation of the spatial distribution of fog droplets by a holographic method. Q.J.R. Meteorol. Soc. 110, 63–73.
Ladoy, P., Lovejoy, S., Schertzer, D., 1991. Extreme variability of climatological data: scaling and intermittency. In: Schertzer, D., Lovejoy, S. (Eds.), Non-linear Variability in Geophysics: Scaling and Fractals. Kluwer Academic Publishers, The Netherlands, pp. 241–250.
Ladoy, P., Schmitt, F., Schertzer, D., Lovejoy, S., 1993. Variabilité temporelle des observations pluviometriques à Nîmes. C.R. Acad. Des. Sci. 317 (II), 775–782.
Lavergnat, J., Golé, P., 1998. A stochastic raindrop time distribution model. J. Appl. Meteorol. 37, 805–818.
Lilley, M., Lovejoy, S., Strawbridge, K., Schertzer, D., 2004. 23/9 dimensional anisotropic scaling of passive admixtures using lidar aerosol data. Phys. Rev. E 70, 036307-1-7.
Lopez, R.E., 1977. The lognormal distribution and cumulus cloud populations. Mon. Weather Rev. 105, 865–872.
Lovejoy, S., 1982. Area-perimeter relation for rain and cloud areas. Science 216, 185–187.
Lovejoy, S., Lilley, M., Desaulniers-Soucy, N., Schertzer, D., 2003. The large particle number limit in Rain. Phys. Rev. E 68, 025301.
Lovejoy, S., Schertzer, D., 1990. Fractals, raindrops and resolution dependence of rain measurements. J. Appl. Meteorol. 29 (11), 1167–1170.
Lovejoy, S., Schertzer, D., 1991. Multifractal analysis techniques of rain and cloud fields from 10^3 to 10^6 m. In: Schertzer, D., Lovejoy, S. (Eds.), Scaling, Fractals and Non-Linear Variability in Geophysics. Kluwer Academic Publishing, Dordrecht, pp. 111–144.
Lovejoy, S., Schertzer, D., 1995. Multifractals and rain. In: Kundzewicz, A.W. (Ed.), New Uncertainty Concepts in Hydrology and Hydrological Modeling. Cambridge University Press, Cambridge, pp. 62–103.
Lovejoy, S., Schertzer, D., 2006. Multifractals, cloud radiances and rain. J. Hydrol. (in press).
Lovejoy, S., Schertzer, D., Tsonis, A.A., 1987. Functional box-counting and multiple elliptical dimensions in rain. Science 235, 1036–1038.
Lovejoy, S., Duncan, M., Schertzer, D., 1996. The scalar multifractal radar observer's problem and rain. J. Geophys. Res. 31D 26, 479–492.
Lovejoy, S., Schertzer, D., Stanway, J.D., 2001. Direct evidence of planetary scale atmospheric cascade dynamics. Phys. Rev. Lett. 86 (22), 5200–5203.
Malinowski, S.P., Zawadzki, I., 1993. On the surface of clouds. J. Atmos. Sci. 50 (1), 5–13.
Marsan, D., Schertzer, D., Lovejoy, S., 1996. Causal space–time multifractal processes: predictability and forecasting of rain fields. J. Geophys. Res. 101 (D21), 26333–26346.
Menabde, M., Harris, D., Seed, A., Austin, G., Stow, D., 1997. Multiscaling properties of rainfall and bounded random cascades. Water Resour. Res. 33 (12), 2823–2830.

Olsson, J., 1995. Limits and characteristics of the multifractal behavior of a high resolution rainfall time series. Nonlinear Process. Geophys. 2 (1), 23–29.

Olsson, J., 1996. Validity and applicability of a scale-independent, multifractal relationship for rainfall. J. Atmos. Sci. 42, 53–65.

Olsson, J., Niemczynowicz, J., 1996. Multifractal analysis of daily spatial rainfall distributions. J. Hydrol. 187, 29–43.

Over, T.M., Gupta, V.K., 1994. Statistical analysis of mesoscale rainfall: dependence of a random cascade generator on large-scale forcing. J. Appl. Meteorol. 33, 1526–1542.

Paluch, I.R., Baumgardner, D.G., 1989. Entrainment and fine-scale mixing in a continental convective cloud. J. Atmos. Sci. 46 (2), 271–278.

Parisi, G., Frisch, U., 1985. On the singularity spectrum of fully developed turbulence. In: Ghil, M., Benzi, R., Parisi, G. (Eds.), Turbulence and Predictability in Geophysical Fluid Dynamics, Amsterdam.

Radkevich, A., Lovejoy, S., Strawbridge, K., Schertzer, D., 2006. 29/9 dimensional space-time atmospheric stratification of passive admixtures using lidar data. Phys. Rev. E (submitted for publication).

Schertzer, D., Lovejoy, S., 1985a. Generalised scale invariance in turbulent phenomena. Physico-Chem. Hydro. J. 6, 623–635.

Schertzer, D., Lovejoy, S., 1985b. Generalized scale invariance and fractal models of rain. Water Resour. Res. 21, 1233–1250.

Schertzer, D., Lovejoy, S., 1987. Physical modeling and analysis of rain and clouds by anisotropic scaling multiplicative processes. J. Geophys. Res. 92, 9693–9714.

Schertzer, D., Lovejoy, S., 1991. Non-linear variability in geophysics: Scaling and Fractals. Kluwer, 318 pp.

Schertzer, D., Lovejoy, S., 1992. Hard and soft multifractal processes. Physica A 185, 187–194.

Schertzer, D., Lovejoy, S., 1997. Universal multifractals do exist!: Comments on ''A statistical analysis of mesoscale rainfall as a random cascade''. J. Appl. Meteor. 36, 1296–1303.

Schertzer, D., Lovejoy, S., Hubert, P., 2002. An introduction to stochastic multifractal fields. In: Ern, A., Weiping, Liu (Eds.), Mathematical Problems in Environmental Science and Engineering, Contemporary Applied Mathematics, vol. 4. Higher Education Press, Beijing, pp. 106–179.

Schmitt, F., Lavallée, D., Schertzer, D., Lovejoy, S., 1992. Empirical determination of universal multifractal exponents in turbulent velocity fields. Phys. Rev. Lett. 68, 305–308.

Seed, A., 1989. Statistical problems in measuring convective rainfall. Ph.D. thesis, McGill University.

Tessier, Y., 1993. Multifractal objective analysis: rain and cloud, Ph.D. thesis, McGill University.

Tessier, Y., Lovejoy, S., Schertzer, D., 1993. Universal multifractals in rain and clouds: theory and observations. J. Appl. Meteorol. 32, 223–250.

Tessier, Y., Lovejoy, S., Schertzer, D., 1994. The multifractal global raingage network: analysis and simulation. J. Appl. Meteorol. 33, 1572–1586.

Tessier, Y., Lovejoy, S., Hubert, P., Schertzer, D., Pecknold, S., 1996. Multifractal analysis and modeling of rainfall and river flows and scaling, causal transfer functions. J. Geophys. Res. 31D, 26427–26440.

Tritton, 1990. An Introduction to Fluid Mechanics. Oxford University Press.

Uijlenhoet, R., Stricker, J.N.M., Torfs, P.J.J.F., Creutin, J.-D., 1999. Towards a stochastic model of rainfall for radar hydrology: testing the Poisson homogeneity hypothesis. Phys. Chem. Earth (B) 24, 747–755.

Venugopal, V., Foufoula-Georgiou, E., Sapozhnikov, V., 1999. Evidence of dynamic scaling in space-time. J. Geophys. Res. 104, 31599–31610.

Zawadski, I., 1995. Is rain fractal? In: Kundzewicz, A.W. (Ed.), New Uncertainty Concepts in Hydrology and Hydrological Modeling. Cambridge University Press, Cambridge, pp. 62–103.